Raman lidar measurements of tropospheric water vapor over Hefei

Yonghua Wu (吴永华), Huanling Hu (胡欢陵), Shunxing Hu (胡顺星), and Jun Zhou (周 军)

Anhui Institute of Optics and Fine Mechanics, Chinese Academy of Sciences, Hefei 230031

Received April 17, 2003

L625 Raman lidar has been developed for water vapor measurements over Hefei, China since September 2000. By transmitting laser beam of frequency-tripled Nd:YAG laser, Raman scattering signals of water vapor and nitrogen molecules are simultaneously detected by the cooled photomultipliers with photon counting mode. Water vapor mixing ratios measured by Raman lidar show the good agreements with radiosonde observations, which indicates this Raman lidar is reliable. Many observation cases show that aerosol optical parameters have the good correlation with water vapor distribution in the lower troposphere.

OCIS codes: 010.3640, 010.7340, 280.3640.

Lidar (light detection and range) developed quickly with the advanced laser and optical-electronic techniques[1]. Its applications in atmospheric remote sensing become more and more important. Comparing with the common observation facilities, lidar measurement has the higher spatial and temporal resolution. It is more important that lidar can continuously get spatial distribution of atmospheric constituents. Water vapor (H_2O) is one of the active and key atmospheric traces. It has the significant infrared absorption effects in the solar-earth radiation, and it is crucial in the cloud formation. Therefore, water vapor plays the great roles in atmospheric radiations and climate changes[2]. But, profile observations of tropospheric water vapor are currently very limited in the meteorological stations, so Raman lidar is a good candidate for measuring tropospheric water vapor distributions, its potential capacity has been demonstrated and validated[3,4]. Raman lidar usually makes tropospheric water vapor observations because Raman scattering returns are $3-4$ order weaker than elastic scattering of particle and molecules, so relative calibration is necessary for lidar systematic constant. Its advantages are that Raman lidar only needs to emit one laser beam and can simultaneously get the aerosol optical parameters with higher accuracy algorithm. Differential absorption lidar (DIAL) for water vapor can attain low stratosphere, which doesnot need other calibration for water vapor profiles, but more complicated laser system is needed[4,5]. In this paper, L625 Raman lidar is described for the nighttime measurements of tropospheric water vapor over Hefei (31.9°N/117.17°E), China.

L625 Raman lidar operates with the frequency-tripled Nd:YAG laser at 355 nm, whose pulse energy is about 60 mJ with repetition rate of 10 Hz and divergence less than 1 mrad. A 62.5-cm diameter Cassegrain telescope is used to collect atmospheric scattering returns from water vapor Raman (407.4 nm), nitrogen Raman (N_2, 386.7 nm), molecule and aerosol (355 nm). A fused silica optical fiber and its couplers guide these light signals into beam-splitters. This fiber has 2-mm core diameter and NA 0.36, which fits with field of view 2 mrad for the receiving optical system. Transmission of fiber is larger than 95% per meter over the range of wavelength $355-532$ nm. Fiber coupler and collimators are designed with all of reflecting mirrors in order to overcoming dichromatic effects of different wavelengths. Backscattering light signals are separated, and then detected by three cooled photomulitipliers (PMTs) for H_2O-Raman (407.4 nm), N_2-Raman (386.7 nm) and elastic scattering (355 nm), respectively. Thorn EMI PMTs operate with temperature -20 °C for decreasing thermal and dark current noises. Interference filters placed in front of PMTs help cut down the background light noise. Barr filters in H_2O-Raman and N_2-Raman channels are the key components for suppressing the cross-talk of elastic scattering (Mie-Rayleigh) returns. Both of them have the block ratio 10^{-12} at wavelength 355 nm and 532 nm. For Raman channels, the transmission values of filter are about 40% at 407.4 nm and 60% at 386.7 nm, respectively. Filter bandwidth with 4.3 nm is considered to overcome the variation of Raman scattering cross-section with different temperature[6]. In the elastic scattering channel, bandpass of interference filter is 1 nm, which has block ratio 10^{-5} for background radiation noise. Considering the saturation and nonlinear effects of detectors caused by over-strong signals from lower altitudes, neutral density filters are usually added in N_2-Raman and elastic scattering channels. Outputs

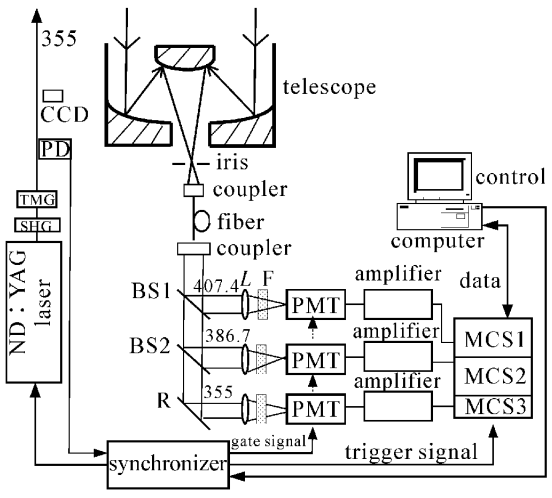

Fig. 1. Schematic diagram of L625 H_2O-Raman lidar. PD: photodiode; L: lens; F: filter; BS: beam-splitter.

Table 1. The Main Specifications of L625 H_2O-Raman Lidar

Transmitter			
Laser	Nd:YAG		
Wavelength (nm)	355		
Pulse Energy (mJ)	60		
PRF (Hz)	10		
Divergence (mrad)	≤ 1		
Receiver			
Telescope	Cassegrain Type		
Diameter	625 mm, $f/7.37$		
FOV	2 mrad		
Optical fiber	ϕ 2 mm, NA: 0.36, 3-m-long, PCS Fiberguide Inc.		
Interference Filter (Barr Associate)			
CW (nm)	407.4	386.7	355
	H_2O-Raman	N_2-Raman	Elastic
Bandwidth (nm)	4.7	4.3	1.0
Transmission (%)	40	60	40
Blocking at 355 nm	10^{-12}	10^{-12}	
PMT(THORN EMI)	9214QB	9214QB	9817B
Preamplifier	VT120B×3		
Gain	200		
Bandwidth	250 MHz		
Data Acquisition and Control			
Photon Counter (EG&G)	T914P (150 MHz)		
Range Resolution	30 m		
Synchronizer			
Computer	PC/Windows		

of PMTs are firstly amplified by the fast preamplifiers, then checked by three multi-channel scalers (MCS, EG&G, and T914P) with maximum counting rate 150 MHz. Because of uncoaxiality of transmitting laser beam and receiver, this lidar can receive the useful signals above 0.6-km altitude. Figure 1 shows the schematic diagram of this Raman lidar. Table 1 lists its main specifications.

Water vapor mixing ratios can be derived from the ratios of H_2O-Raman to N_2-Raman scattering signals. Systematic constant ratio of two Raman channels is calibrated by best-fitting lidar data with radiosonde measuring data[7]. Routine radiosonde observations have been made twice every month over Hefei, so we can periodically check the variability of calibration constant. Differential transmissions at H_2O-Raman and N_2-Raman shift wavelength are corrected by aerosol extinction obtained with N_2-Raman and elastic scattering signals. We also add N_2-Raman filter in H_2O-Raman channel to correct optical alignment differences between two Raman channels[3]. L625 Raman lidar currently makes the regular nighttime measurements at Hefei. One signal profile is recorded with integrated laser shots 5000 and spatial resolution 30 meters. In order to reduce the uncertainty caused by photon counting fluctuation and noise, water vapor mixing ratio distributions are obtained by integrating the returns of laser shots 40,000, and the raw signals are running-smoothed with range of 300 m below 3-km altitude and 600 m above 3-km altitude.

Figure 2(a) shows water vapor mixing ratio profiles obtained by L625 Raman lidar and GZZ-59 type radiosonde on September 13, 2001. Figure 2(b) presents their relative differences. Short bars in Fig. 2(a) indicate the statistic errors of L625 Raman lidar measurements, and they are usually less than 5% below 6-km altitude, 15% between 6- and 9-km altitude. Water vapor profile of Raman lidar agrees well with the radiosonde data. Generally, their discrepancies are less than 20% except the altitude range of 2.6 – 3.9 km and 7.3-km altitude in Fig. 2(b), where it is relatively dry air layer. Water vapor mixing ratios of Raman lidar show drier than radiosonde results. Two factors probably contribute to these differences. One is that the humidity sensor of GZZ-59 radiosonde has large measuring errors in lower moisture air (relative humidity < 20%). Systematic biases of GZZ-59 radiosonde are usually between 5%–10% under the mid-high moisture conditions, even worse at the temperature below 0 °C by comparing with RS-80 and VIZ-1392 radiosonde[8]. Intercomparisons of different types of radiosondes already found that humidity measurements had larger differences than temperature and pressure observations. Intercomparisons of water vapor profiles by other Raman lidar and radiosonde also demonstrate this situation[7,9]. Therefore, higher accuracy humidity sensor of radiosonde is greatly expected

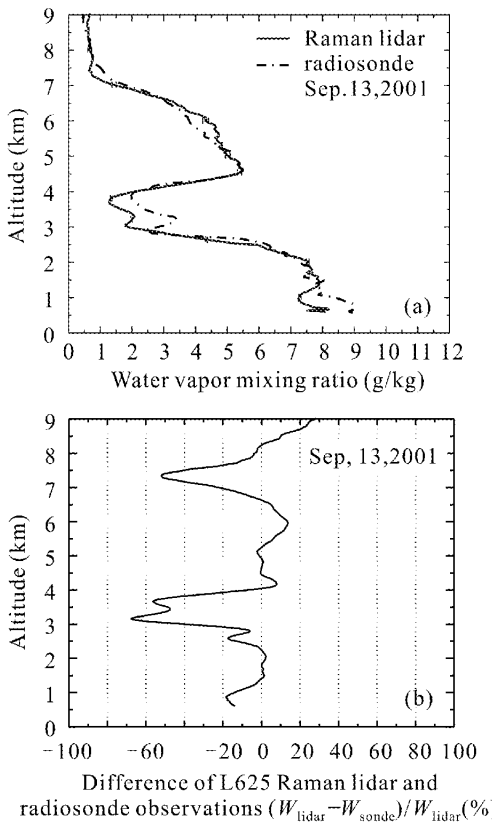

Fig. 2. (a) Water vapor mixing ratio distributions measured by Raman lidar and radiosonde, and (b) their differences.

for calibrating H_2O-Raman lidar data. Other factor is the differences of measuring time and ambient air by Raman lidar and radiosonde. Usually, L625 Raman lidar gives the one-hourly mean of water vapor distribution in the vertical point of lidar, but GZZ-59 radiosonde gives the transient humidity at some altitudes on its ascending pathways.

Figures 3(a) and (b) present other example of water vapor mixing ratios obtained by Raman lidar and radiosonde on June 6, 2002. Short bars in Fig. 3(a) represent the statistic errors of water vapor measured by L625 Raman lidar. Water vapor distributions of Raman lidar are consistent with one of radiosondes between 0.6 and 7 km. Figure 3(b) shows that most of their relative differences are less than 20%. Figures 4(a) and (b) illustrate other two profiles of water vapor mixing ratios observed by L625 Raman lidar and radiosonde, they are coincident with each other. In summertime, this Raman lidar measurements can attain higher altitudes because of higher moisture. On the contrary, it only attains 5-km altitude due to lower humidity in wintertime. From the results above, we can find that rich water vapor exists below 2-km altitude over Hefei, but other moisture layer sometimes can be found above 3-km altitude (see Figs. 2 and 4). Sharp gradients of water vapor distribution appear between 2- and 3-km altitude, which are correlated to the thermal and dynamic process in the planetary boundary layer.

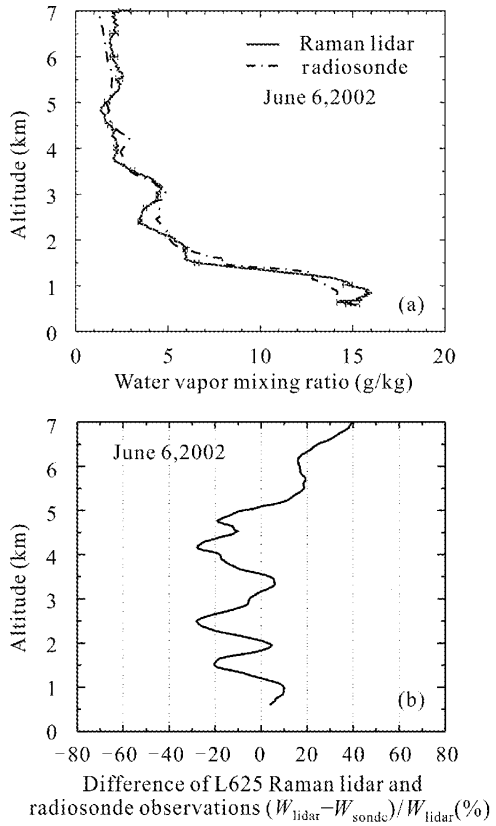

Fig. 3. (a) Water vapor mixing ratio distribution measured by Raman lidar and radiosonde, and (b) their differences.

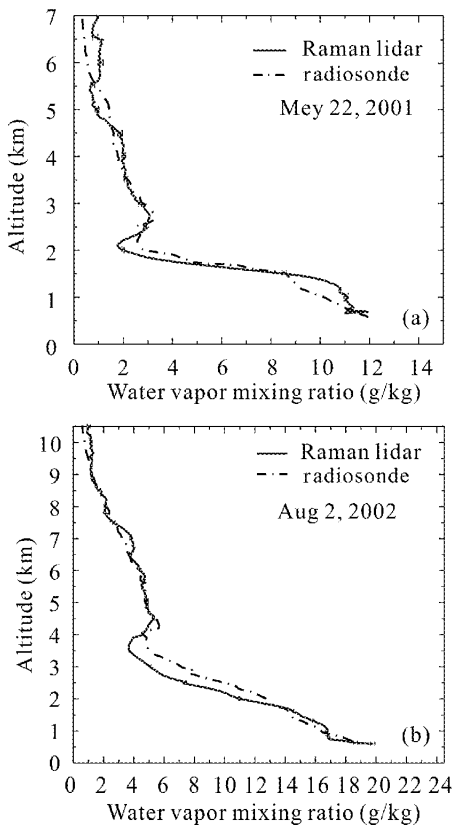

Fig. 4. Water vapor mixing ratio distribution measured by L625 Raman lidar and radiosonde.

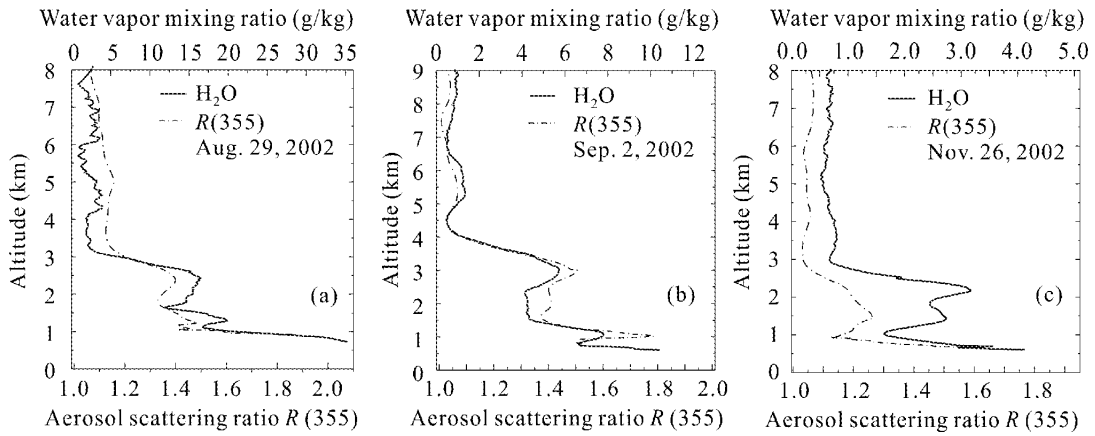

Fig. 5. Aerosol and water vapor distribution profiles measured by L625 Raman lidar over Hefei.

L625 Raman lidar can simultaneously measure water vapor and aerosol distribution. Our observations frequently indicated that the distribution of aerosol optical parameters showed good correlation with the distribution of water vapor mixing ratios. Figure 5 plots water vapor and aerosol scattering ratios distributions at 355 nm obtained by L625 Raman lidar in the different days. It is clear that similar structures of aerosol and water vapor mixing ratios appear below 3-km altitude. Other Raman lidar also found these correlations between water vapor and aerosol optical properties[10]. It can be understood that high moisture makes the hygroscopic aerosol particles grow, and refractive index of aerosol will be also changed[11], which probably results in aerosol optical properties changing. These interesting relationships need further observations and analysis.

This paper reports one Raman lidar for tropospheric water vapor and aerosol measurements at Hefei, China. Typical profiles of water vapor distributions are obtained by this Raman lidar. By comparing with radiosonde observations, their coincident results demonstrate that performances and measurements of this Raman lidar are reliable. Some measuring cases show that aerosol optical properties are probably influenced by water vapor in the lower altitudes. Regular observations of this Raman lidar will further contribute to study the statistic distribution characteristics of water vapor and its influences in aerosol optical properties over Hefei.

This work was supported by the National 863 high technology research project. The authors wish to recognize Mr. Fudi Qi, Guming Yue, Jisheng Xu and Chen Li for their contributions to the development of this Raman lidar. Mr. Chengsheng Ma performs radiosonde observations. Y. WU's e-mail address is wyh@aiofm.ac.cn.

References

1. M. P. McCormick, in *Advances in Atmospheric Remote Sensing with Lidar* A. Ansmann, R. Neuber, R. Rairoux, and U. Wandinger, (ed.) (Springer-Verlag, Berlin, 1996) p. 141.
2. E. K. Schneider, B. P. Kirtman, and R. S. Lindzen, J. of Atmos. Sci. **56,** 1649 (1999).
3. D. N. Whiteman, S. H. Melfi, and R. A. Ferrare, Appl. Opt. **31,** 3068 (1991).
4. W. B. Grant, Opt. Eng. **30,** 40 (1991).
5. G. Ehret, K. P. Hoinka, J. Stein, A. Fix, C. Kiemle, and G. Poberaj, J. Geophys. Res. **104,** 31351 (1999).
6. D. N. Whiteman, W. F. Murphy, N. W. Walsh, and K. D. Evans, Opt. Lett. **18,** 247 (1993).
7. R. A. Ferrare, S. H. Melfi, D. N. Whiteman, K. D. Evans, F. J. Schmidlin, and D. O'C. Starr, J. Atmos. Oceanic Technol. **23,** 1177 (1995).
8. A. C. Zhang, B. L. Zhao, (ed.) *Modern Meteorological Observations* (in Chinese) (Beijing University Press, Beijing, 2000) p. 300.
9. J. Weseel, S. M. Beck, Y. C. Chan, R. W. Farley, and J. A. Gelbwachs, IEEE Trans. Geoscience and Remote Sensing **38,** 141 (2000).
10. T. Sakai, T. Shibata, and Y. Iwasaka, J. of Meteoro. Soc. of Japan **75,** 1179 (1997).
11. G. Hänel and M. Lehmann, Contrib. Atmos. Phys. **54,** 57 (1981).